I&EC research
Industrial & Engineering Chemistry Research

REVIEW

pubs.acs.org/IECR

An Overview of the Liquid−Liquid Equilibria of (Ionic Liquid + Hydrocarbon) Binary Systems and Their Modeling by the Conductor-like Screening Model for Real Solvents

Ana R. Ferreira,[†] Mara G. Freire,[†] Jorge C. Ribeiro,[‡] Fernando M. Lopes,[‡] João G. Crespo,[§] and João A. P. Coutinho*,[†]

[†]Departamento de Química, CICECO, Universidade de Aveiro, Campus Universitário de Santiago, 3810-193 Aveiro, Portugal

[‡]Galp Energia, Refinaria de Matosinhos, Rua Belchior Robles, 4452-852 Leça da Palmeira, Matosinhos, Portugal

[§]CQFB/REQUIMTE, Departamento de Química, FCT, Universidade Nova de Lisboa, 2829-516 Caparica, Portugal

Supporting Information

ABSTRACT: Ionic liquids (ILs), with their unique and tunable properties, are attracting the interest of both academia and refining companies as potential solvents for the extraction of specific compounds from hydrocarbons' streams. For such a purpose, the knowledge of the mutual solubilities between ionic liquids and hydrocarbons is required. Experimental measurements for all these systems are impracticable due to the large number of possible combinations of ionic liquids and hydrocarbons. Thus, a deeper understanding of the interactions taking place, and ruling the phase behavior, and the development of predictive models are essential issues to forecast a general picture of the liquid−liquid equilibria (LLE) between ionic liquids and hydrocarbons. In this work an overview of the mutual solubilities between ionic liquids and hydrocarbons is presented. A review of the experimental data available is reported, and the effect of various structural features of both the ionic liquids and the hydrocarbons through their mutual solubilities behavior is discussed. The capability of the Conductor-like Screening Model for Real Solvents (COSMO-RS) to predict the LLE of (IL + hydrocarbon) binary systems is further evaluated. More than 150 binary systems were investigated. It is shown that COSMO-RS allows a semiquantitative description of the LLE experimental data for the systems studied. Moreover, COSMO-RS majorly provides a correct qualitative trend of the phase behavior dependence of the ionic liquids and molecular compounds. Therefore, COSMO-RS can be a useful predictive tool with great potential in the screening of ionic liquids for specific extraction applications.

1. INTRODUCTION

Ionic liquids (ILs) are a new class of solvents that have been object of a growing interest from both academia and industry in the past few years. They are molten salts composed by bulky organic cations, and organic or inorganic anions, which form crystalline structures with low lattice energies, allowing these salts to be in the liquid state at or near room temperature. Ionic liquids exhibit, in general, negligible vapor pressures, often possess high thermal and chemical stabilities, and have good solvating capacity for both organic and inorganic compounds, among others unique properties. Given the huge number of possible ionic liquids, their properties can be fine-tuned by an adequate combination of specific ions and/or functional groups, making of them "designer solvents" that could be tailored to fit the requirements of a specific process.

The interesting properties of ionic liquids are commending their application in numerous chemical and industrial processes, aiming at replacing conventional organic solvents, including chemical, catalytic and biological reactions,[1,2] organic/inorganic synthesis,[3−5] liquid−liquid separation processes,[6−8] separation and purification of gases[9,10] and contaminants removal from aqueous streams.[11] There are some industrial processes that already use ionic liquids due to their economical advantages and reaction yields,[12,13] such as the BASIL (Biphasic Acid Scavenging utilizing Ionic Liquids) process,[14−16] proposed by BASF technologies, and the Difasol process,[17,18] developed by Institute Français du Pétrole (IFP) that is an improvement of the traditional Dimersol route.

Refining companies belong to an industrial sector that has shown a considerable interest in ionic liquids. Various separation processes relevant for refineries have been studied, namely the desulfurization of fuels,[19−24] the selective separation of aromatic/aliphatic hydrocarbon mixtures,[6,7,25−27] and extractive distillation.[12,28] Besides the ionic liquids enhanced performance on these separations, their low volatility can reduce the energy consumption to separate the solvents from the product streams and to regenerate them.[6,29] To evaluate the applicability of ionic liquids in these processes the large body of experimental data of various ionic liquids with a broad range of hydrocarbons that has been reported[30−50] is detailed and reviewed below.

To identify the improved ionic liquids to be used in particular applications it is necessary to know their thermophysical properties and to understand the phase behavior of systems containing such ionic fluids. This cannot be accomplished using only the

Received: December 10, 2010
Accepted: March 9, 2011
Revised: February 28, 2011
Published: March 29, 2011

available experimental data due to the very large number of possible combinations of ionic liquids and hydrocarbons that undergo liquid−liquid phase equilibria. It is thus necessary to develop a comprehensive understanding of the impact of the hydrocarbon molecules features (such as aromaticity, chain length, and cyclization of aliphatic hydrocarbons), as well as of the ionic liquids structural changes impact (cation and anion nature, alkyl side chain length, and additional functional groups) on their phase behavior. The development and testing of predictive models able to describe the phase behavior of systems containing ionic liquids can produce an important tool for this purpose.

A number of models based on the excess Gibbs free energy have been applied on the modeling of the phase behavior of systems involving ionic liquids and hydrocarbons. Some classical local composition models, such as the non-random two liquid (NRTL)[31,32,35,36,38−43,45,50−53] and UNIQUAC,[35,40,51] were applied with success to the description of these systems while their performances were shown to be similar.[35,40,51] The modified Flory−Huggins equation and a lattice model based on polymer-solution models have also been applied,[30,54] yielding good quantitative descriptions of the phase diagrams. Although the models employed in these studies provide improved correlations, they present a limited predictive capability since they require parameters fitted to previous experimental data and to the ionic liquid complex groups. A fully predictive alternative lays in the use of the Conductor-like Screening Model for Real Solvents (COSMO-RS) proposed by Klamt and co-workers.[55−57] COSMO-RS does not require adjustable parameters, and therefore, it is applicable to virtually all possible ionic liquids and hydrocarbons mixtures. COSMO-RS has already been applied by Domańska et al.[33] in the description of the equilibrium of (ILs + hydrocarbon) systems. Albeit reasonable results were obtained,[33] the limited number of systems studied was insufficient for a detailed evaluation of the COSMO-RS performance and applicability.

In the current work, a review of the experimental data published hitherto, concerning the mutual solubilities of hydrocarbons and ionic liquids, is carried out to garner a broader picture of the structural changes of both hydrocarbons and ionic liquids toward their phase behavior. Aiming at appraising a predictive model for the screening and design of ionic liquids for task specific applications involving hydrocarbons, the performance of COSMO-RS in the description of the (ILs + hydrocarbons) liquid−liquid equilibria (LLE) is further evaluated.

2. IONIC LIQUID + HYDROCARBON LIQUID−LIQUID EQUILIBRIA

An extensive search was performed on the liquid−liquid equilibrium experimental data of ionic liquids and hydrocarbons binary systems available in literature. The ionic liquid and hydrocarbon used, measurement technique, temperature, and composition ranges, as well as the respective literature reference, are summarized in Tables S1−S3 in Supporting Information. Table S1 reports systems regarding aliphatic hydrocarbons, Table S2 concerns aromatics hydrocarbons, and Table S3 summarizes the available data involving cyclic hydrocarbons.

Owing to the high expectation through the application of ionic liquids in petroleum refineries and fuel production a large number of experimental systems could be found, with ionic liquids ranging from the most common types to task specific compounds. The experimental data available are based on imidazolium, pyridinium, pyrrolidinium, ammonium, and phosphonium cations, and bis(trifluoromethylsulfonyl)imide, alkylsulfate, hexafluorophosphate, tetrafluoroborate, thiocyanate, tosylate, nitrate, dicyanamide, and trifluoromethanesulfonate anions. Their ionic structures are described in Table 1 and Table 2. LLE measurements were carried out for the *n*-alkanes pentane, hexane, heptane, octane, nonane, decane, and hexadecane; for the aromatics benzene, toluene, ethylbenzene, propylbenzene, butylbenzene, *o*-xylene, *m*-xylene, and *p*-xylene; and for the cycloalkanes cyclopentane, cyclohexane and cycloheptane.

The large bank of experimental data gathered allows the drawing of the solvents structural features ruling the solvation phenomenon and the evaluation of the performance of COSMO-RS in anticipating their solution behavior.

3. COSMO-RS

COSMO-RS[55,57−59] is a model for the prediction of thermophysical properties and phase behavior of pure fluids and/or mixtures, that combines quantum chemistry, based on the dielectric continuum model known as COSMO (COnductor-like Screening MOdel for Real Solvents), with statistical thermodynamics cycles to reduce the thermodynamics of the mixture to the interaction of a mixture of individual surface segments (chemical potential determination).

COSMO calculations are performed in a perfect/ideal conductor,[55,57−59] that is, molecules are assumed as surrounded by a virtual conductor environment, and the interactions are completely made on the conductor interface, taking into account the electrostatic screening and the back-polarization of the solute molecule. As result, it provides a discrete surface around the solute molecule which is characterized by its geometry and screening charge density (σ) that iteratively corresponds to a minimum energetic state at the conductor. COSMO-RS treats the surface around the solute molecule as segments, and it also similarly treats the screening charge density of the respective segment, σ'. These data are stored in the so-called COSMO files.

In the molecular interaction approach, the electrostatic misfit energy, E_{misfit}, and the hydrogen bounding energy, E_{HB}, are the most relevant strengths and are described as a function of the polarization charges of the two interacting segments, (σ, σ') or (σ_{acceptor},σ_{donor}). The van der Waals energy is also taken into account but in an approximate way that only depends on the element type of the atoms involved. These energies are described by eqs 1, 2, and 3, respectively:

$$E_{\text{misfit}}(\sigma,\sigma') = a_{\text{eff}}\frac{\alpha'}{2}(\sigma+\sigma')^2 \quad (1)$$

$$E_{\text{HB}} = a_{\text{eff}}c_{\text{HB}}\min(0;\min(0;\sigma_{\text{donor}}+\sigma_{\text{HB}}) \times \max(0;\sigma_{\text{acceptor}}-\sigma_{\text{HB}})) \quad (2)$$

$$E_{\text{vdW}} = a_{\text{eff}}(\tau_{\text{vdW}}+\tau'_{\text{vdW}}) \quad (3)$$

There are five adjustable parameters fitted to the individual atoms properties: a_{eff} is the effective contact area between two surface segments; α' is an interaction parameter; C_{HB} is the hydrogen bond strength; σ_{HB} is the threshold for hydrogen bonding; and τ_{vdW} and τ'_{vdW} are element specific van der Waals interaction parameters.

COSMO-RS does not explicitly depend on the discrete surface geometry; thus, the 3D density distribution on the surface of each solute molecule X_i is converted into a distribution function

Table 1. Abbreviations and Chemical Structure of the Cations Studied

abbreviation	description	chemical structure
$[C_1mim]^+$	1,3-dimethylimidazolium	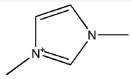
$[C_2mim]^+$	1-ethyl-3-methylimidazolium	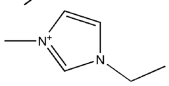
$[C_4mim]^+$	1-butyl-3-methylimidazolium	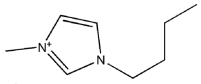
$[C_6mim]^+$	1-hexyl-3-methylimidazolium	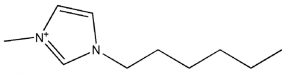
$[C_8mim]^+$	1-methyl-3-octylimidazolium	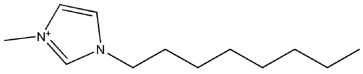
$[C_6H_{13}OCH_2mim]^+$	1-hexyloxymethyl-3-ethylimidazolium	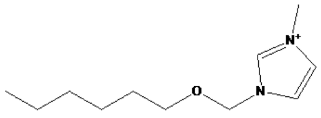
$[(C_6H_{13}OCH_2)_2im]^+$	1,3-dihexyloxymethyl-imidazolium	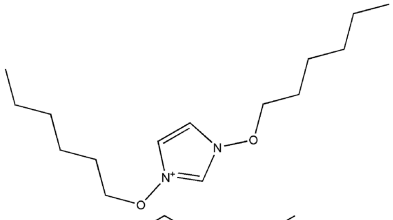
$[1,3C_4mpy]^+$	1-butyl-3-methylpyridinium	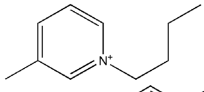
$[1,4C_4mpy]^+$	1-butyl-4-methylpyridinium	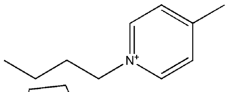
$[C_4mpyr]^+$	1-butyl-1-methylpyrrolidinium	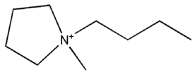
$[P_{i(444)1}]^+$	tri-*iso*-butyl(methyl)phosphonium	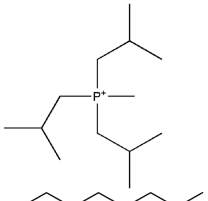
$[P_{666\,14}]^+$	trihexyl(tetradecyl)phosphonium	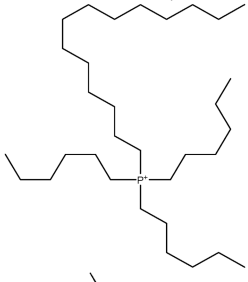
$[N_{22(OH)11}]^+$	ethyl(2-hydroxyethyl)dimethylammonium	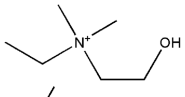
$[N_{62(OH)11}]^+$	hexyl(2-hydroxyethyl)dimethylammonium	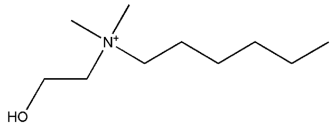
$[N_{101011}]^+$	didecyldimethylammonium	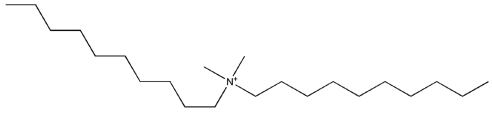

dx.doi.org/10.1021/ie102471b |*Ind. Eng. Chem. Res.* 2011, 50, 5279–5294

Table 2. Abbreviations and Chemical Structure of the Anions Studied

abbreviation	description	chemical structure
$[MeSO_4]^-$	methylsulfate	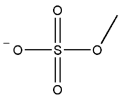
$[EtSO_4]^-$	ethylsulfate	
$[OcSO_4]^-$	octylsulfate	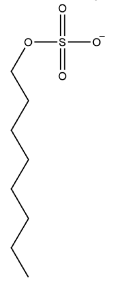
$[PF_6]^-$	hexafluorophosphate	
$[BF_4]^-$	tetrafluoroborate	
$[NTf_2]^-$	bis[(trifluoromethyl)sulfonyl]imide	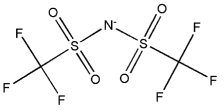
$[TOS]^-$	tosylate	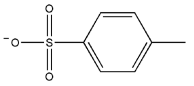
$[NO_3]^-$	nitrate	
$[SCN]^-$	thiocyanate	
$[DCA]^-$	dicyanamide	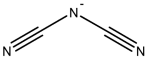
$[CF_3SO_3]^-$	trifluoromethanesulfonate	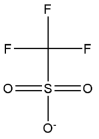
$[MDEGSO_4]^-$	2-(2-methoxyethoxy)ethylsulfate	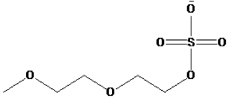
$[Ac]^-$	acetate	

called σ-profile, $p^X(\sigma)$. This distribution function describes the relative amount of surface segment with polarity σ. The combination of the molecular σ-profiles with the pure or mixture solvents (S) σ-profiles results in the mole fraction weighted sum

dx.doi.org/10.1021/ie102471b |*Ind. Eng. Chem. Res.* 2011, 50, 5279–5294

of σ-profiles of its compounds, $p_S(\sigma)$, that normalized by the total surface area, A_S, gives the normalized σ-profile of the overall system, $p'_S(\sigma)$:

$$p'_S(\sigma) = \frac{p_S(\sigma)}{A_S} = \frac{\sum_i x_i p^{X_i}(\sigma)}{\sum_i x_i A^{X_i}} \quad (4)$$

where x_i is the mole fraction of component i, $p^{X_i}(\sigma)$ is the corresponding σ-profile, and A^{X_i} is surface area of the solute molecule X_i.

Since $p'_S(\sigma)$ describes the molecular interactions, the chemical potential can be estimated by solving iteratively eq 5 while coupling $p'_S(\sigma)$ with the energies associated to the molecular interactions:[59]

$$\mu_S(\sigma) = -\frac{RT}{a_{eff}} \ln\left[\int p_S(\sigma') \exp\left(\frac{1}{RT}(a_{eff}\mu_S(\sigma') - E_{misfit}(\sigma,\sigma') - E_{HB}(\sigma,\sigma'))\right) d\sigma'\right] \quad (5)$$

where $\mu_S(\sigma)$, known as σ-potential, is the chemical potential of a surface segment with screening charge density σ, and it is a measure of the affinity of a solvent S to the surface segment with polarity σ.

Integrating eq 6 described below, over the surface of a compound, makes it possible to calculate the pseudochemical potential of the component X_i in a solvent S:[57]

$$\mu_S^{X_i} = \mu_{C,S}^{X_i} + \int p^{X_i}(\sigma)\, \mu_S(\sigma)\, d\sigma \quad (6)$$

where $\mu_{C,S}^{X_i}$ is a combinatorial contribution of different sizes and shapes of molecules in the mixture.

This set of COSMO-RS equations gives the chemical potential of all components of a mixture and allows the estimation of several thermodynamic properties, namely activity coefficients, partition coefficients, VLE, and LLE, among others.[57−61]

The LLE of hydrocarbons + ILs binary systems were studied as a function of temperature using the quantum chemical COSMO calculation performed in the Turbomole program package[62,63] with the BP (Becke-Perdew) density functional theory and the Ahlrichs-TZVP (triple-ζ valence polarized large basis set),[64] employing the parameter file BP_TZVP_C2.1_0110. Moreover, the pseudobinary approach, inputting the ionic liquid cation and anion as isolated species with the same mole fraction, was used along all the COSMOtherm calculations. The chemical potentials were determined for each factual ternary system (IL cation + IL anion + hydrocarbon) while the chemical potential of the ionic liquid is the sum of the isolated ions chemical potentials.

Since ionic liquids are complex molecules, they present different conformational geometries corresponding to various energy states. In a previous work, Freire et al.[61] studied the conformers influence in the LLE description of ionic liquids and alcohols systems and concluded that improved results are obtained using the conformers with lower energies (energetically more stable). In this work, the COSMO-RS calculations were performed with the lower energy state conformers of each IL anion, IL cation, and hydrocarbon.

4. RESULTS AND DISCUSSION

The systems reported in Tables S1, S2, and S3 in the Supporting Information were used to study the effect of the various structural characteristics of the hydrocarbons molecules (such as aromaticity, chain length, cyclization, and positional isomerism) and of the ionic liquids (cation core and anion nature, side alkyl chain length, and additional functionalized groups) on their phase behavior. A detailed discussion through the structural features impact in the phase behavior of these systems is reported below. It should be remarked that the solubility data from different researchers/sources show some discrepancies for similar systems.[30,33,35] This fact could derive from the different experimental techniques used, purities of the compounds employed, among others sources of error.[30,33,35] In this work a critical evaluation of the experimental data was carried out by comparing similar systems and, whenever outsider results were observed, they were not considered in the following discussion.

The COSMO-RS model was applied to the description of selected systems to evaluate its capacity to predict the phase equilibrium data experimentally available. The impact of structural factors of the solvents on the miscibility gap of the LLE diagrams are analyzed and discussed.

4.1. Hydrocarbons + ILs Binary Systems. Fixing a common ionic liquid in several systems allows the investigation of the differences between the mutual solubilities regarding various hydrocarbon families. Data for [C_4mim][SCN] with hexane, cyclohexane, and benzene are reported in Figure 1 (for other ionic liquids see Figures S1−S16 in Supporting Information). The asymmetric behavior of the ionic-liquid-containing systems is one of the most striking features of these diagrams. As previously observed with alcohols[61] and water[65] the solubility of ILs in hydrocarbons is usually orders of magnitude lower (in a mole fraction basis) than the solubility of hydrocarbons in ionic liquids. Particularly, while at the IL-rich phase the solubility of hydrocarbons is quite substantial, at the hydrocarbon-rich phase the solubility of [C_4mim][SCN] is very small. Moreover, the solubility of benzene in aromatic ionic liquids, such as the imidazolium-based ionic liquid presented in Figure 1, is significantly higher than that observed for the aliphatic hydrocarbons. Nevertheless, slight differences also exist in the solubilities of both aliphatic hydrocarbons studied and the ionic liquid. Generally, the mutual solubilities between hydrocarbons (with a constant carbon number) and ionic liquids follow the increasing order (*cf.* also Supporting Information): aromatics > cyclic aliphatic hydrocarbons > *n*-alkanes. The large solubility of aromatic hydrocarbons in ILs is certainly related to the formation of $\pi-\pi$ interactions between the aromatic rings of both ionic liquid ions and aromatic hydrocarbons. On the other hand, the cyclic conformation of aliphatic hydrocarbons can reduce steric hindrance and allows a more effective package of the hydrocarbon at the IL-rich phase.

COSMO-RS predictions for the phase behavior of the studied systems are also depicted in Figure 1. COSMO-RS displays an enhanced performance in describing all systems containing the ionic liquid [C_4mim][SCN]. Besides the qualitative trend description, improved quantitative results are also obtained. Nevertheless, COSMO-RS is not able to achieve consistently predictions of this quality for all ionic liquids evaluated (*cf.* Supporting Information). However, in general, a semiquantitative description of the phase diagrams is achieved, with the model being able to describe the differences between the various types of hydrocarbons. Particularly, the large differences in the mutual solubilities with ionic liquids displayed between the aromatics and aliphatic hydrocarbons are usually well described. As previously observed,[60,61,65]

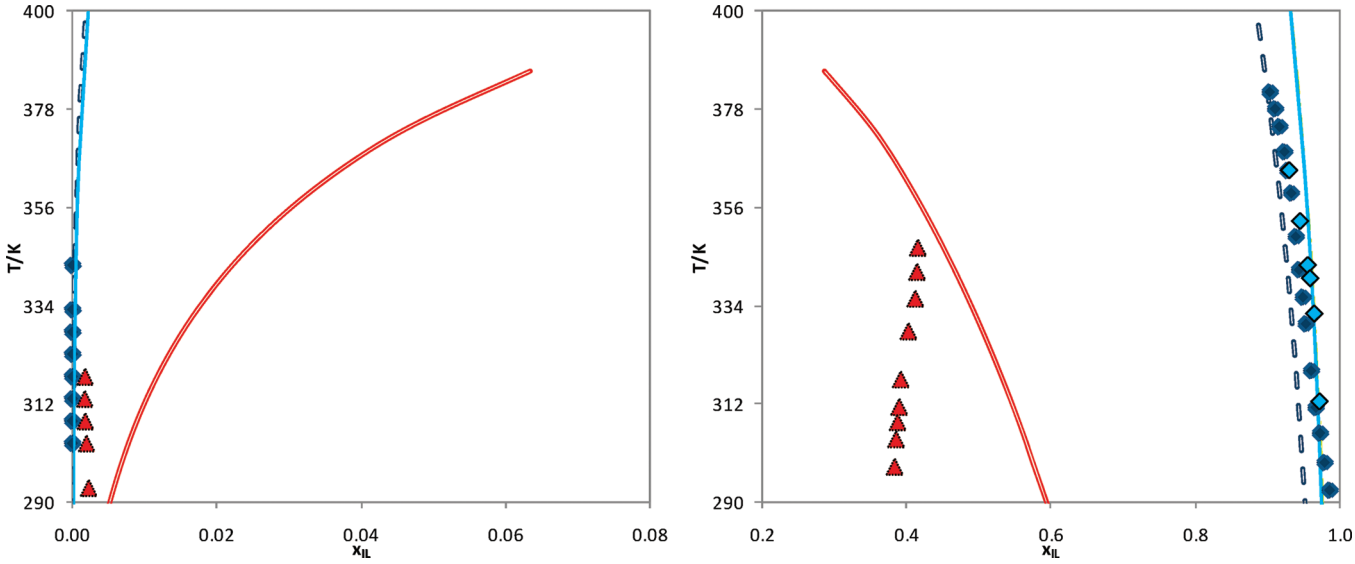

Figure 1. Liquid−liquid phase diagram for [C_4mim][SCN] with *n*-hexane[32] (light blue diamonds, solid line), benzene[32] (red triangles, double solid line), and cyclohexane[32] (dark blue diamonds, double dashed line). The symbols and the lines represent, respectively, the experimental data and the COSMO-RS prediction calculations.

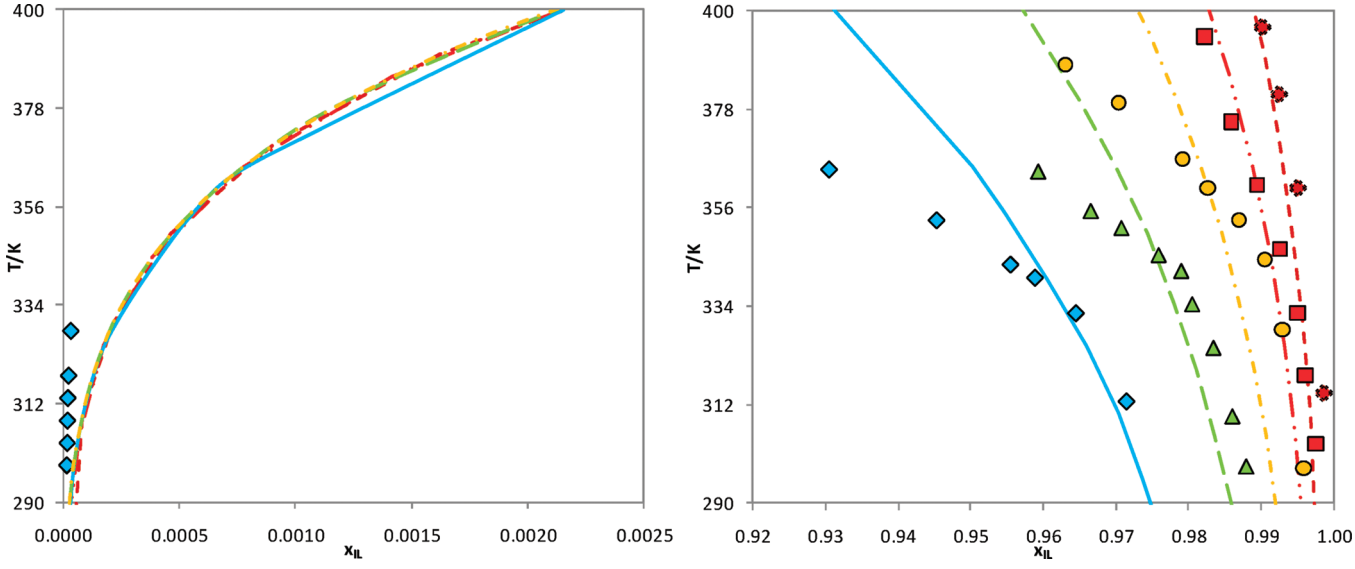

Figure 2. Liquid−liquid phase diagram for [C_4mim][SCN] with *n*-hexane[32] (light blue diamonds, solid line), *n*-heptane,[32] (green triangles, long dashed line), *n*-octane,[32] (orange circles, dot-dash line), *n*-nonane[32] (red squares, dash-dot-dot line) and *n*-decane[32] (red crosses, short dashed line). The symbols and the lines represent, respectively, the experimental data and the COSMO-RS prediction calculations.

the COSMO-RS model performs better for less miscible systems. Since COSMO-RS calculations consider that the interactions are made on the conductor interface surrounding the molecules (thus isolated species), stronger interactions responsible for larger mutual solubilities are not adequately taken into account by COSMO-RS.

4.2. *n*-Alkanes + ILs Binary Systems. As described in Supporting Information, in Table S1, a large number of measured systems of *n*-alkanes + ILs is available. The LLE data taken from the literature are, in general, based on *n*-alkanes from C_5H_{12} to $C_{10}H_{22}$ and, in most examples, only data for the solubility of the *n*-alkanes at the ionic-liquid-rich regime are available. The experimental measurements of the solubility of ionic liquids in *n*-alkanes are a challenging task since the equilibrium saturation values of ILs in *n*-alkanes are very small—in the range of 1×10^{-5} to 3×10^{-5} in mole fraction for the reported systems.[36,38,51] Moreover, the solubility of *n*-alkanes in ionic liquids is extremely low, compared, for instance, with aromatic hydrocarbons, due to the striking strength differences of the type of interactions that take place between the hydrocarbons (dispersion forces) and the ionic liquid ions (mainly hydrogen bonding and electrostatic interactions).

4.2.1. Effect of the n-Alkane Chain Length upon the Phase Behavior. Fixing the ionic liquid, the *n*-alkane influence in the liquid−liquid phase diagram of systems of the type IL + *n*-alkane was studied and selected LLE diagrams are shown in Figure 2, and in Supporting Information (Figures S17−S36).

The increase of the *n*-alkane chain length increases the immiscibility of the binary system, as shown in Figure 2 for [C_4mim][SCN].

The increasing miscibility gap increases accordingly to the rank: *n*-decane < *n*-nonane < *n*-octane < *n*-heptane < *n*-hexane. This trend is found to be independent of both the ionic liquid cation and anion nature. Although an increase in the dispersive forces is expected between the alkyl chains of the ionic liquids and longer chain hydrocarbons, the decrease in solubility at the IL-rich phase is related with the difficulty that *n*-alkanes with higher chains meet to fit into the free volume between the ionic liquid ions, reducing therefore their packing efficiency.[34] As can be extrapolated from Figure 2, as well as from Supporting Information Figures S17−S36, the alkane chain length increase leads to an increase in the upper critical solution temperature (UCST) of all the binary systems evaluated. Indeed, dealing with aliphatic hydrocarbons, all diagrams converge to an UCST behavior.

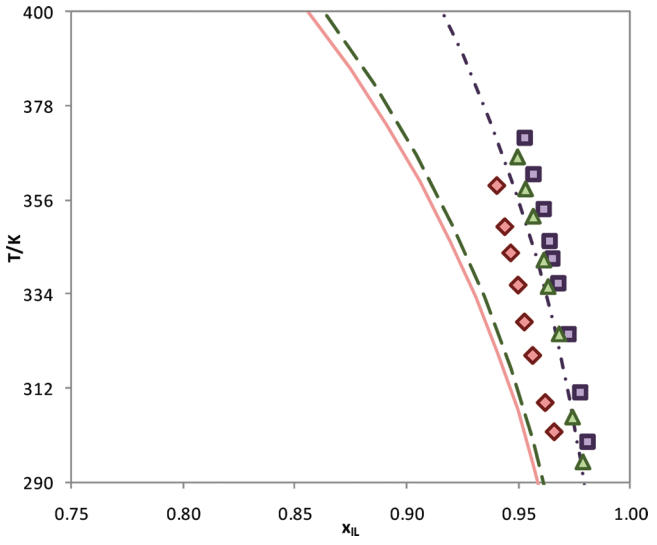

Figure 3. Liquid−liquid phase diagram for $[C_4mim][CF_3SO_3]$[50] (purple squares, dot-dash line), $[C_4mpyr][CF_3SO_3]$[50] (green triangles, dashed line), and $[1,3\text{-}C_4mpy][CF_3SO_3]$[50] (pink diamonds, solid line) with *n*-hexane. The symbols and the lines represent, respectively, the experimental data and the COSMO-RS prediction calculations.

The liquid−liquid equilibria of [SCN]-based ionic liquids presented in Figure 2 and Figure S24 is quantitatively described by COSMO-RS regarding the alkane chain length effect. For systems with different ionic liquids, with higher miscibility among the binary compounds, a fair qualitative description of the solubilities was obtained as displayed in Supporting Information, Figures S17−S34. For the hydrocarbon-rich phase, no experimental data are available, and thus, COSMO-RS predictions were not attempted.

4.2.2. Effect of the Ionic Liquid Cation Core upon the Phase Behavior. The effect of the ionic liquid cation core on the solubility of hydrocarbons in ionic liquids is depicted in Figure 3 and Figure 4 where the solubilities of *n*-hexane in $[CF_3SO_3]$- and [TOS]-based ionic liquids are presented. The solubilities seem to be highly anion dependent. Nevertheless, a remarkable effect of the cation family is also observed when comparing, for instance, significantly structural different ionic liquids, such as all, nitrogen-based ILs with the phosphonium-based ionic liquid. The results displayed in Figures 3 and 4 show that the increasing miscibility of *n*-alkanes in ionic liquids follows the cations trend: $[1,3\text{-}C_4mpy]^+ < [C_4mpyr]^+ < [C_4mim]^+ \ll [P_{i(444)1}]^+$. Among the nitrogen-based ionic liquids the five-sided ring cations (imidazolium- and pyrrolidinium-based) present lower miscibilities with *n*-alkanes compared to the six-sided ring cation studied (pyridinium-based ionic liquid). Since both pyridinium- and imidazolium-based ionic liquids present an aromatic character while the pyrrolidinium-based cation is aliphatic, it can be anticipated that the IL cation size is more relevant than the presence of π molecular orbitals in defining the mutual solubilities. The most significant differences in solubilities, among different ionic liquid cations, were observed with the phosphonium-based ionic liquid, as shown in Figure 4, presenting a significantly smaller miscibility envelope. The phosphonium-based structure, based on four alkyl chains, leads to favorable dispersive interactions with *n*-alkanes than those observed with other families of ionic liquids with a more polar character, thus increasing the mutual solubilities.

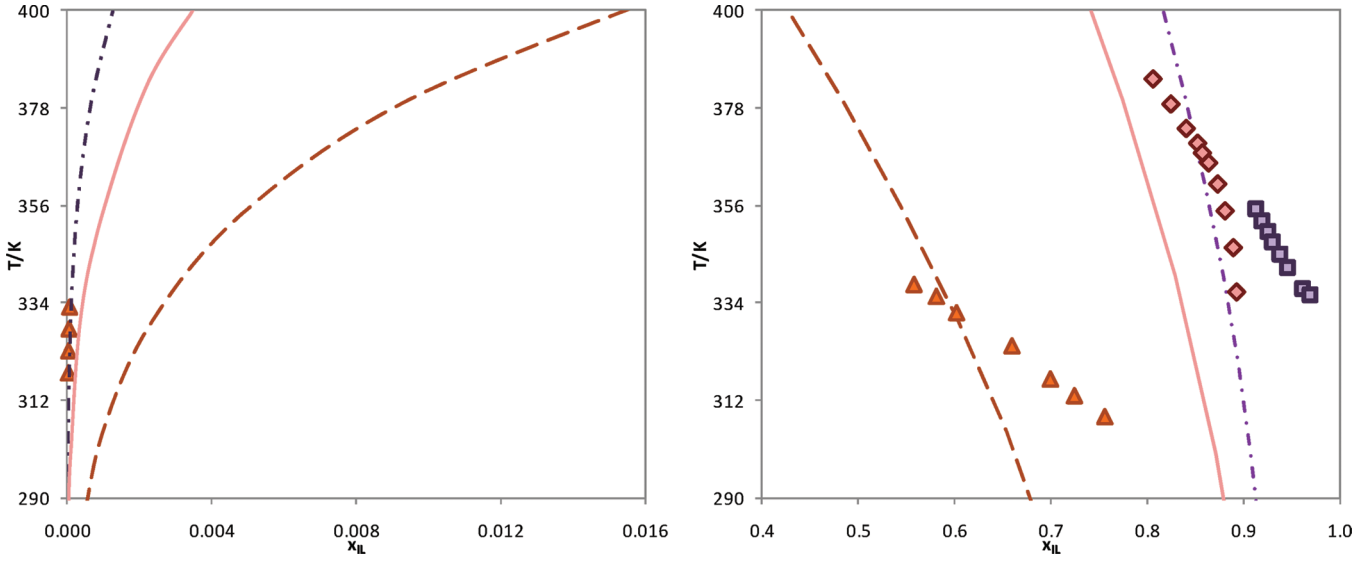

Figure 4. Liquid−liquid phase diagram for $[C_4mim][TOS]$[36] (purple square, dot-dash line), $[1,4C_4mpy][TOS]$[49] (pink diamonds, solid line) and $[P_{i(444)1}][TOS]$[47] (orange triangles, long dashed line) with *n*-hexane. The symbols and the lines represent, respectively, the experimental data and the COSMO-RS prediction calculations.

dx.doi.org/10.1021/ie102471b |*Ind. Eng. Chem. Res.* 2011, 50, 5279–5294

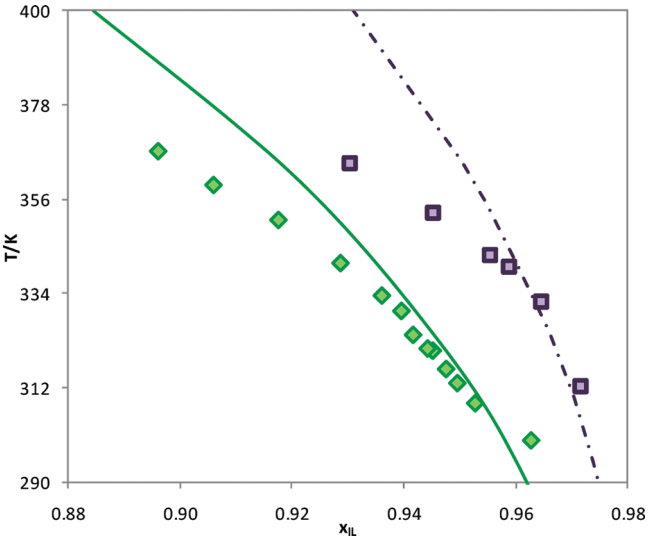

Figure 5. Liquid−liquid phase diagram for $[C_4mim][SCN]$[32] (purple squares, dot-dash line) and $[C_6mim][SCN]$[38] (green diamonds, solid line) with *n*-hexane. The symbols and the lines represent, respectively, the experimental data and the COSMO-RS prediction calculations.

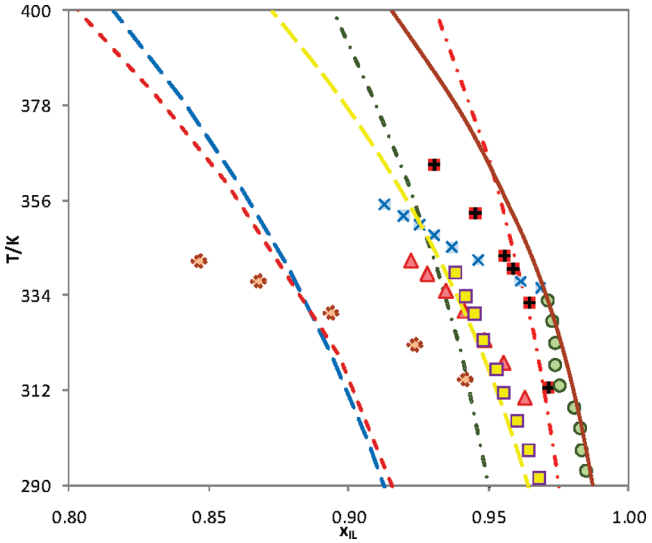

Figure 6. Liquid−liquid phase diagram for $[C_4mim][MeSO_4]$[35] (green circles, double dot-dash line), $[C_4mim][PF_6]$[51] (orange diamonds, solid line), $[C_4mim][SCN]$[32] (red crossed squares, dot-dash line), $[C_4mim][TOS]$[36] (blue X, long dashed line), $[C_4mim][CF_3SO_3]$[50] (yellow squares, double long dashed line) and $[C_4mim][MDEGSO_4]$[39] (red triangles, short dashed line) with *n*-hexane. The symbols and the lines represent, respectively, the experimental data and the COSMO-RS prediction calculations.

COSMO-RS can satisfactorily predict the solubility dependency with the cation family as can be seen in Figures 3 and 4 (as well as for other systems presented in Supporting Information, Figures S36−S39).

4.2.3. Effect of the Ionic Liquid Cation Alkyl Chain Length upon the Phase Behavior. The cation alkyl chain length affects the mutual solubilities between ionic liquids and *n*-alkanes. Indeed, the chain length has a significant impact on the phase diagrams as shown in Figure 5. Figure 5 show that the increase of the ionic liquid cation alkyl chain from $[C_4mim]^+$ to $[C_6mim]^+$ in the $[C_nmim][SCN]$ series leads to an increase in the mixture solubility. This enhanced miscibility is the result of a free volume increase in the IL-rich solution and of the prevalence of nonpolar regions in the ionic liquid that enhance the probability of favorable dispersive interactions with the *n*-alkane chain. Curiously this trend is not observed when changing the ionic liquid anion for the systems containing $[C_1mim][MeSO_4]$ and $[C_4mim][MeSO_4]$ (see Figures S40 and S41 in Supporting Information). Nevertheless, it is difficult at present to establish if this is a peculiar behavior related with the $[C_1mim]^+$ cation, the $[MeSO_4]^-$ anion, or just a problem associated with the limited experimental data available. More data on these systems are required to establish the reasons behind this particular trend.

Moreover, for the alkoxymethyl-based ionic liquids ($C_nH_{2n+1}OCH_2$) a similar pattern was observed. As shown in Supporting Information, in Figure S44, *n*-alkanes are more soluble in $[(C_6H_{13}OCH_2)_2im][NTf_2]$ than in $[C_6H_{13}OCH_2mim][NTf_2]$ at similar temperatures. The substitution of a methyl group by a longer alkoxymethyl chain improves the miscibility with aliphatic hydrocarbons. Most of the imidazolium-based ionic liquids phase diagrams shown presented *n*-alkanes solubilities lower than 0.30 in mole fraction units. For the cations with the hexyloxy-groups, the *n*-alkane solubility increases up to 0.5 in mole fraction. Nevertheless, with the data published hitherto it is not possible to conclude if this is a direct effect of the increased polarity of the chain dominated by the alkoxy group or a simple contribution of the second and longer hexyl chain.

The trend observed with the cation alkyl chain length is similar to that observed for alcohol + IL binary systems.[61] Also, as the alkyl chain length of the cation increases the UCST of the system decreases. Moreover, the opposite effect verified with the *n*-alkanes chain length increase, leading to higher UCST, is similar to that presented by alcohols and ionic liquids systems.[61]

COSMO-RS provides a correct qualitative description of the experimental data of the systems studied in Figure 5 (and Supporting Information Figures S43 and S44). The effect of the increase in the cation chain length leading to higher mutual miscibilities is well predicted. It should be remarked that this trend is also supported by COSMO-RS for the systems comprising the methylsulfate-based ionic liquids, although experimentally a different pattern was observed.

4.2.4. Effect of the Ionic Liquid Anion upon the Phase Behavior. The experimental data available (Supporting Information, Table S1) allow a comparison of the effect of several ionic liquid anions on the *n*-alkanes solubility in the ionic media. Although more data are available, as described in Table S1, the systems here analyzed are mainly based on the $[C_4mim][anion]$ + *n*-hexane and the $[C_6H_{13}OCH_2mim][anion]$ + *n*-hexane systems, because they allow the direct comparison of the effect of a large number of anions on the mutual solubilities. Results are displayed in Figure 6 and Supporting Information (Figure S46).

The ionic liquid anion nature has a slight influence in the mutual solubilities and similar to that presented before with the ionic liquid cation core. The main deviation was observed with the IL containing the $[PF_6]^-$ anion. Experimentally, the solubility of *n*-alkanes in $[C_4mim]$-based ionic liquids increases with the following order: $[MeSO_4]^- < [SCN]^- < [TOS]^- < [CF_3SO_3]^- < [MDEGSO_4]^- \ll [PF_6]^-$, while for $[C_6H_{13}OCH_2mim]$-based ionic liquids the increasing solubility follows the rank: $[BF_4]^- < [NTf_2]^-$. These patterns closely follow the hydrogen bond basicity (hydrogen-bond accepting strength) of

dx.doi.org/10.1021/ie102471b |*Ind. Eng. Chem. Res.* 2011, 50, 5279–5294

[C_4mim]-based ionic liquids regarding their anions. The hydrogen bond basicity, the β solvatochromic parameter, accordingly to the ionic liquid anion nature follows the sequence $[MeSO_4]^-$ > $[SCN]^-$ > $[CF_3SO_3]^-$ > $[BF_4]^-$ > $[PF_6]^-$ > $[NTf_2]^-$.[66,67] Thus, it seems that the solubility of *n*-alkanes in ionic liquids decreases with an increase of the hydrogen-bond basicity of the ionic liquid anion. It should be noted that no liquid−liquid equilibrium data were found regarding the influence of the ionic liquid anion at the hydrocarbon-rich phase.

As previously observed for other systems containing ionic liquids,[61,65] the solubility dependence with the anions nature is not qualitatively well described by COSMO-RS. Because of the similarity on the solubilities observed for most anions, although COSMO-RS can often provide an acceptable prediction of the phase diagrams, it cannot identify the correct experimental solubility trends as shown in Figure 6 for the ionic liquids [C_4mim][$MeSO_4$], [C_4mim][PF_6], and [C_4mim][TOS]. Nevertheless, in Supporting Information, Figure S46, concerning only the $[NTf_2]^-$ and $[BF_4]^-$ anions, there is a close qualitative agreement with experimental data.

4.2.5. Effect of the Ionic Liquid Anion Alkyl Chain Length upon the Phase Behavior. As discussed before, the increase in the cation alkyl chain length leads to a pronounced increase in the mutual miscibility between ILs and *n*-alkanes. The same trend is observed with the increase of the anion alkyl chain length displayed in Figure 7. Ranging from [C_4mim][$MeSO_4$] to [C_4mim][$OcSO_4$]-containing systems there is a solubility increase of around 0.5 in mole fraction. Such enhanced solubility results from the decrease in the polarity of the anion and from the increase of the dispersion forces between longer alkyl chain anions and *n*-alkanes. In Supporting Information, Figure S47, a similar pattern is observed. [C_4mim][$MeSO_4$] is less soluble in *n*-hexane than [C_4mim][$MDEGSO_4$]. Although an oxygenated group is introduced in the former ionic liquid, this ionic liquid possesses a longer alkyl chain that favors liquid−liquid miscibility.

Despite the limitations of COSMO-RS to describe the ionic liquid anion effect through the binary phase diagrams, as discussed above, the influence of the anion alkyl chain length is correctly described. However, the observed experimental differences in solubilities are more remarkable than those predicted by COSMO-RS.

4.3. Aromatics + ILs Binary Systems. The LLE data available in literature for binary systems containing aromatic hydrocarbons and ionic liquids are reported in Supporting Information, in Table S2. These systems are based essentially in benzene, alkyl-substituted benzenes, and xylene isomers. The experimental miscibility gap observed for the IL + aromatic hydrocarbons is smaller than with *n*-alkanes, the aromatics being much more soluble in ionic liquids. Nevertheless, the solubility of ionic liquids in the aromatics is still very low, in the order of 10^{-3} in mole fraction.[32,36,38,41,46,51,53,68] These important solubility differences observed between aromatics and alkanes in ionic liquids are the basis of the use of ionic liquids for aromatic/aliphatic selective separations.[6,7,25,69,70] The greater solubility of aromatics in ionic liquids can be a consequence of the enhanced interactions between ionic liquids and aromatic hydrocarbons due to $\pi-\pi$ interactions (for aromatic ionic liquids) and favorable packing effects (for nonaromatic ionic liquids). The various structural effects of aromatic hydrocarbons and ionic liquids on the mutual solubilities will be studied and discussed below.

4.3.1. Effect of the Aromatics Structure on the Phase Behavior. The solubility of the ionic liquid in hydrocarbons increases with their aromaticity. As the alkylation of the benzene ring increases, the solubility of the ionic liquid at such a rich phase decreases, as shown in Figure 8 (similar results are also shown in the Supporting Information for other systems in Figure S50 to Figure S91). In general, the miscibility gap increases accordingly to benzene < toluene < ethylbenzene < propylbenzene.

The solubility of xylene isomers in ionic liquids depends on the second methyl group position as shown in Figure 9 for [C_4mim][$MeSO_4$] and for other systems presented in Supporting Information, Figures S50−S91. The small differences observed among the positional isomers are due to differences in the

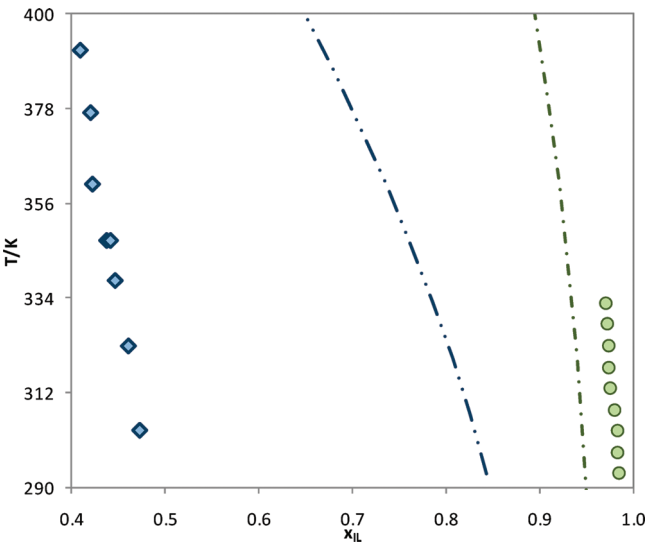

Figure 7. Liquid−liquid phase diagram for [C_4mim][$MeSO_4$][35] (green circles, dot-dash line) and [C_4mim][$OcSO_4$][37] (blue diamonds, dash-dot-dot line) with *n*-hexane. The symbols and the lines represent, respectively, the experimental data and the COSMO-RS prediction calculations.

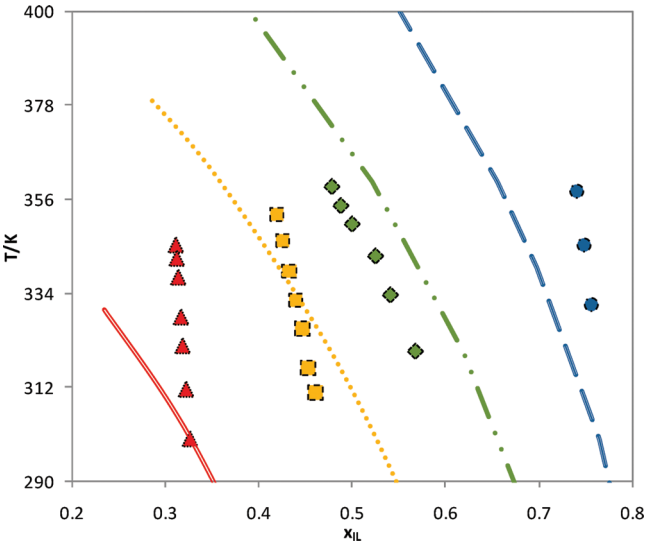

Figure 8. Liquid−liquid phase diagram for [C_4mim][TOS] with benzene[36] (red triangles, double solid line), toluene[36] (yellow squares, dotted line), ethylbenzene[36] (green diamonds, dot-dash line), and propylbenzene[36] (blue circles, long dashed line). The symbols and the lines represent, respectively, the experimental data and the COSMO-RS prediction calculations.

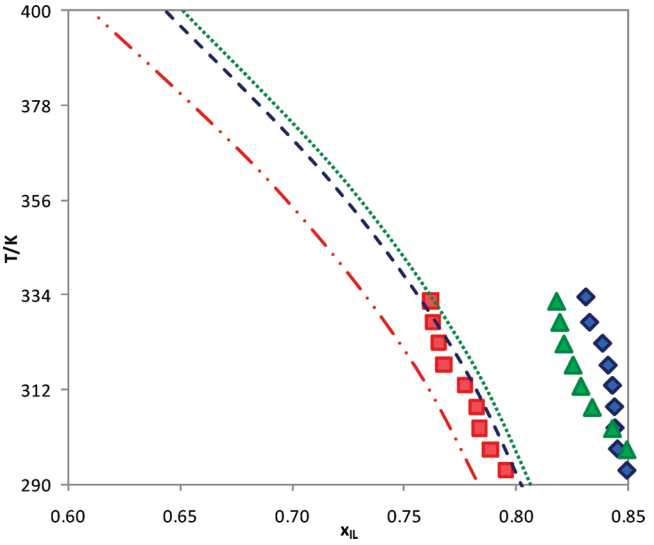

Figure 9. Liquid−liquid phase diagram for $[C_4mim][MeSO_4]$ with *o*-xylene[35] (red squares, dot-dot-dash line), *m*-xylene[35] (blue diamonds, dashed line) and *p*-xylene[35] (green triangles, dotted line). The symbols and the lines represent, respectively, the experimental data and the COSMO-RS prediction calculations.

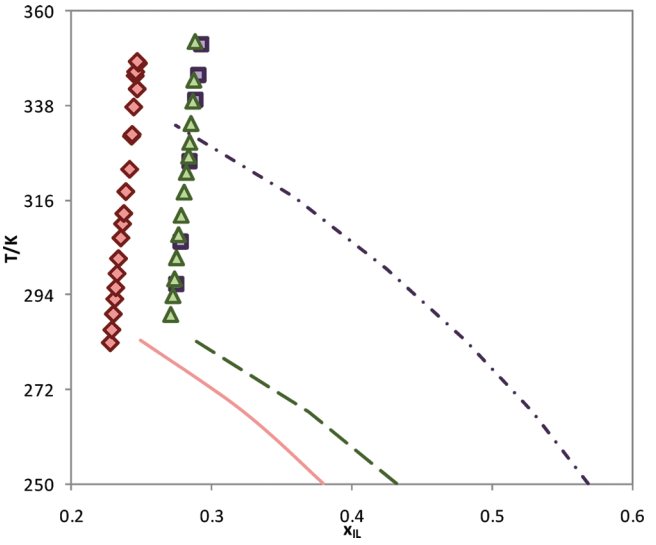

Figure 10. Liquid−liquid phase diagram for $[C_4mim][CF_3SO_3]$[50] (purple squares, dot-dash line), $[C_4mpyr][CF_3SO_3]$[50] (green triangles, long dashed line) and $[1,3\text{-}C_4mpy][CF_3SO_3]$[50] (pink diamonds, solid line) with benzene. The symbols and the lines represent, respectively, the experimental data and the COSMO-RS prediction calculations.

xylene molecular structure that have an impact in the aromatic induced dipole moment. As a result, and in general, the *ortho* compound presents higher solubility at the IL-rich phase.

Moreover, from all the data gathered in Figures 8 and 9, the favorable solvation of ethylbenzene at the IL-rich solution over the xylene similar structures can be seen. A single alkyl chain at the ring allows an enhanced solubility in the ionic liquid as a consequence of its larger dipole moment.

For the hydrocarbon aromatic systems, COSMO-RS is able to qualitatively describe the effect of the alkylation of the benzene ring on the miscibility gap between ionic liquids and aromatics, as shown in Figure 8. Similar results are reported for other systems at the Supporting Information (Figures S50−S91).

The behavior of the xylene isomers systems predicted by COSMO-RS, although only semiquantitative, is qualitatively correct, as shown in Figure 9. The COSMO-RS can predict the similar experimental solubilities observed for the isomers *meta* and *para*, while providing higher miscibilities at the IL-rich phase for the *o*-xylene isomer.

4.3.2. Effect of the Ionic Liquid Cation Core upon the Phase Behavior. As discussed for the IL + *n*-alkane systems, the cation family plays a minor role on the mutual miscibilities when the cation is based on nitrogen-containing heterocyclic rings. Imidazolium-, pyridinium-, and pyrrolidinium-based ionic liquids exhibit similar solubilities as shown in Figure 10. However, pyridinium-based ionic liquids are slightly more soluble in aromatic hydrocarbons and, as observed before, with *n*-alkanes. Other types of cation may however present a different behavior, as suggested by the data for the $[P_{i(444)1}][TOS]$ displayed in Figure 11, which presents a large solubility with aromatic hydrocarbons.

In all systems evaluated, COSMO-RS can satisfactorily predict the trend of the influence of the cation family on the mutual solubilities, as shown in Figures 10 and 11. Nevertheless, significant quantitative differences were observed between the experimental and predicted data. Contrary to what was observed for *n*-alkanes, COSMO-RS predicts more significant differences in solubilities between the imidazolium, the pyridinium, and the pyrrolidium

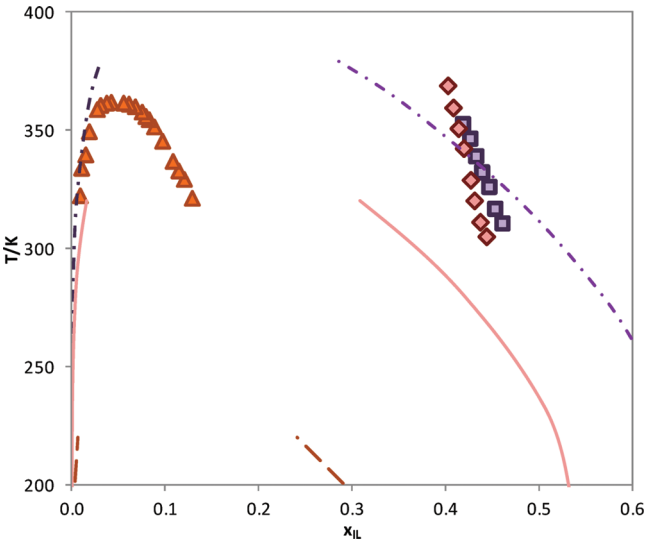

Figure 11. Liquid−liquid phase diagram for $[C_4mim][TOS]$[36] (purple squares, dot-dash line), $[1,4C_4mpy][TOS]$[49] (pink diamonds, solid line), and $[P_{i(444)1}][TOS]$[47] (red triangles, long dashed line) with toluene. The symbols and the lines, represent, respectively, the experimental data and the COSMO-RS prediction calculations.

cations, than those experimentally observed. Again, and as observed before with *n*-alkanes, COSMO-RS predicts an inversion in the solubility trends between the pyridinium- and pyrrolidinium-based ionic liquids at the hydrocarbon-rich phase. Moreover, the experimental data suggest that a number of IL + aromatic systems may have a phase diagram of the lower critical solution temperature (LCST) type (for instance, $[C_4mim][CF_3SO_3]$,[50] $[1,3C_4mpy][CF_3SO_3]$,[50] and $[C_4mpyr][CF_3SO_3]$[50] presented in Figure 10, as well as other systems, such as $[C_2mim][NTf_2]$,[46] $[C_4mim][SCN]$,[32] and $[C_6mim][SCN]$[38] presented in Supporting Information, Figures S60, S5, and S78). In all systems COSMO-RS seems to be unable to describe correctly this particular behavior, predicting

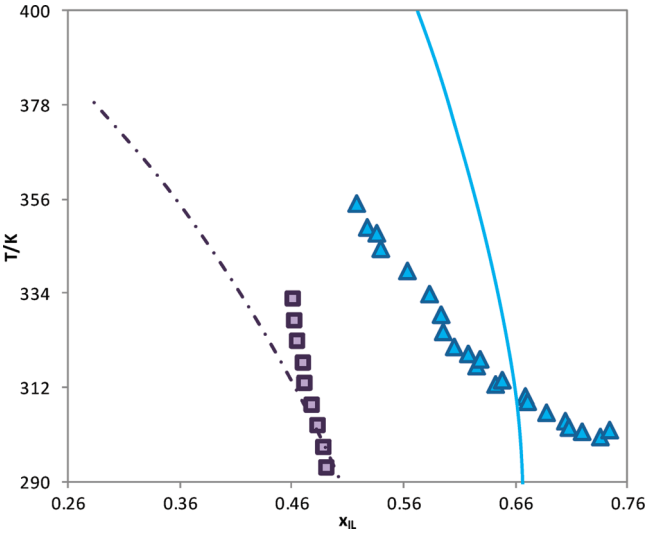

Figure 12. Liquid−liquid phase diagram for $[C_1mim][MeSO_4]$[33] (blue triangles, solid line) and $[C_4mim][MeSO_4]$[35] (purple squares, dot-dash line) with benzene. The symbols and the lines represent, respectively, the experimental data and the COSMO-RS prediction calculations.

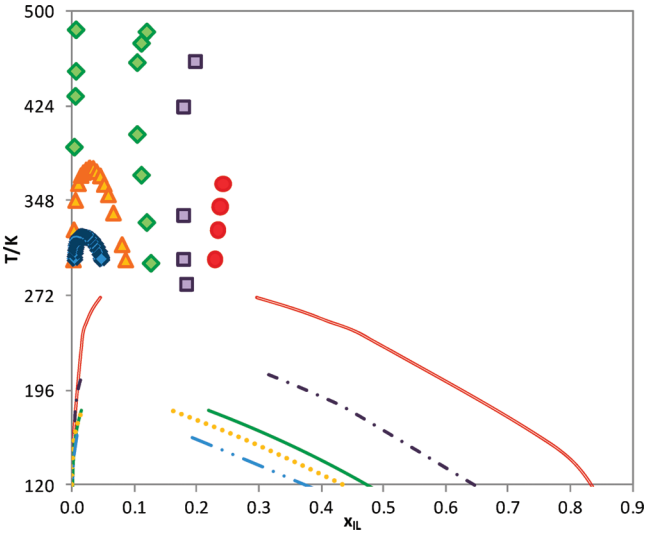

Figure 13. Liquid−liquid phase diagram for $[C_2mim][NTf_2]$[46] (red circles, double solid line), $[C_4mim][NTf_2]$[46] (purple squares, dot-dash line), $[C_6mim][NTf_2]$[46] (green diamonds, solid line), $[C_8mim][NTf_2]$[46] (orange triangles, dotted line) and $[C_{10}mim][NTf_2]$[46] (blue diamonds, dot-dot-dash line) with benzene. The symbols and the lines represent, respectively, the experimental data and the COSMO-RS prediction calculations.

UCST diagrams instead. LCST is caused by the conjugation of attractive interactions and free volume effects which result in negative enthalpies of mixing, and these are not well described by COSMO-RS predictions.

The COSMO-RS predictions usually deteriorate with the increasing miscibility between the compounds.[61,65] For the systems here studied, the COSMO-RS model does not seem to describe correctly the $\pi-\pi$ interactions between aromatic rings. The COSMO-RS calculations consider that the interactions are made at the interface of the virtual conductor environment surrounding the molecules, and stronger interactions responsible for larger mutual solubilities are thus not adequately taken into account. This makes the model less able to describe the aromatic containing systems as compared to the *n*-alkanes systems presented previously. Nevertheless, the model always provides a qualitative description of the ionic liquid cation influence on the mutual solubilities and can be an *a priori* screening tool for particular systems.

4.3.3. Effect of the Ionic Liquid Cation Alkyl Chain Length upon the Phase Behavior. The cation alkyl chain length has an important impact on the solubility of aromatic hydrocarbons in ionic liquids as shown in Figures 12 and 13. The increase of the alkyl chain length decreases the polarity of the ionic liquid cation enhancing favorable interactions with the hydrocarbon. Moreover, the alkyl chain length also increases the entropic effects that contribute to an enhanced solubility, such as the asymmetry and the free volume of the ionic liquid. Figure S104 in Supporting Information shows the effect of the addition of a hexyloxy-group to the imidazolium cation and its impact in the liquid−liquid equilibrium with benzene. The presence of a more polar and electronegative element, such as oxygen, increases the miscibility between the aromatic and the ionic liquid.

Although the COSMO-RS predictions presented in Figures 12 and 13 are quite different from experimental data they can, even so, correctly predict the miscibility trends with the cation alkyl chain length. The only limitation observed in this section was the inability of COSMO-RS to predict the alkoxymethyl group effect on the systems solubility shown in Supporting Information, Figure S104.

4.3.4. Effect of the Ionic Liquid Anion upon the Phase Behavior. The anion effect on the mutual solubilities between aromatic hydrocarbons and ionic liquids is a well studied field with a large body of data available as described in Supporting Information, Table S2. As shown in Figure 14 the ionic liquid anion has a more important influence on the mutual solubilities with aromatic hydrocarbons than that observed before with *n*-alkanes.

The solubility of benzene in the $[C_4mim]$- and $[C_2mim]$-based ionic liquids, shown in Figure 14, and Supporting Information, Figures S105 and S109, range from 0.4 to 0.8 in mole fraction. The solubility increases with the ionic liquids anions sequences: $[MeSO_4]^- < [SCN]^- < [MDEGSO_4]^- < [PF_6]^- < [TOS]^- < [CF_3SO_3]^- < [NTf_2]^-$ for the $[C_4mim]$-based ionic liquids and $[EtSO_4]^- < [PF_6]^- < [NTf_2]^-$ for the $[C_2mim]$-based ionic liquids. In Supporting Information, Figure S109, the solubility with an IL containing a 2-(2-methoxyethoxy)ethyl group at the cation increases as follows: $[BF_4]^- < [NTf_2]^-$. These patterns follow, with few exceptions, the general trend for the dipolarity/polarizability measurements of ionic liquids (π^*): $[MeSO_4]^- \approx [SCN]^- > [BF_4]^- > [PF_6]^- > [CF_3SO_3]^- > [NTf_2]^-$.[67] Thus, the mutual solubilities of aromatic hydrocarbons and ionic liquids increase with the decrease of the polarity of the ionic liquid anion.

The COSMO-RS predictions are quantitatively acceptable for a number of ionic liquids but, as observed before for the *n*-alkanes, the correct qualitative trend predictions present some limitations with the ionic liquid anion nature.

4.4. Cycloalkanes + ILs Binary Systems. The LLE of binary mixtures of IL + cycloalkanes available in literature are based in C_5, C_6, and C_7 cycloalkanes and are summarized in Supporting Information, Table S3. In general, the solubilities of these compounds in ionic liquids are slightly larger than those observed for *n*-alkanes due to their lower molecular volume and cyclic structure responsible by a more effective packing effect. As discussed before, for the solubility of the ionic liquids in other hydrocarbons, the solubility in cycloalkanes is also very small,

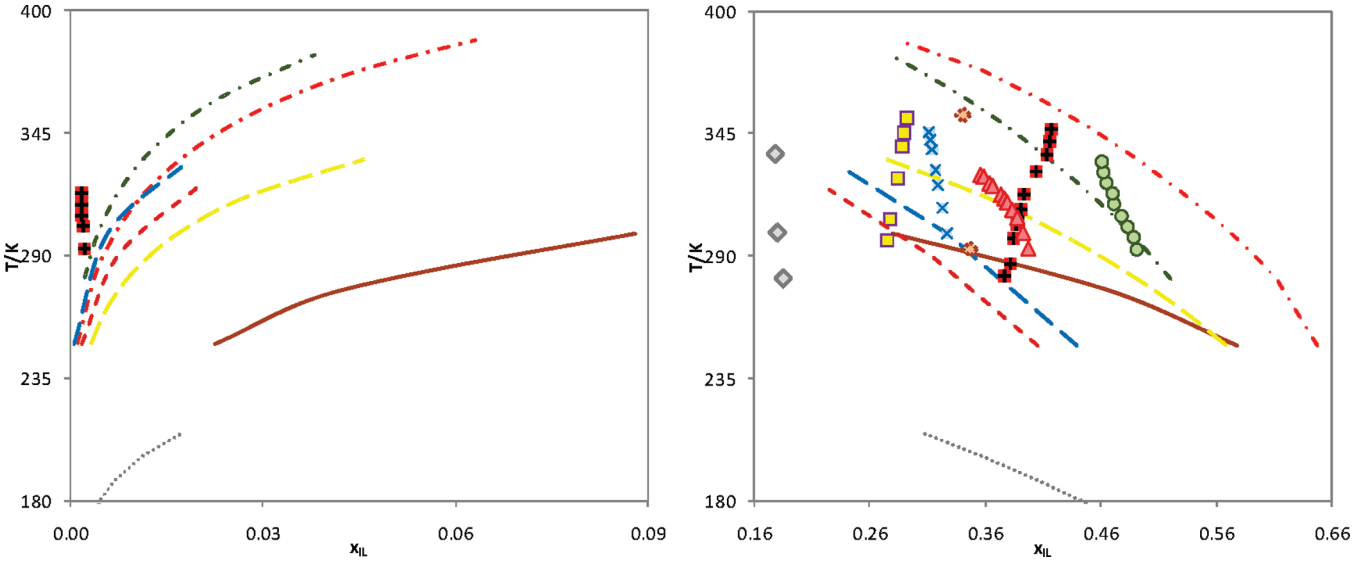

Figure 14. Liquid−liquid phase diagram for $[C_4mim][MeSO_4]$[35] (green circles, double dot-dash line), $[C_4mim][PF_6]$[51] (orange diamonds, solid line), $[C_4mim][NTf_2]$[46] (gray diamonds, dotted line), $[C_4mim][SCN]$[32] (red crossed squares, dash-dot line), $[C_4mim][TOS]$[36] (blue X, dashed line), $[C_4mim][CF_3SO_3]$[50] (yellow squares, double long dashed line) and $[C_4mim][MDEGSO_4]$[39] (pink triangles, dashed line) with benzene. The symbols and the lines represent, respectively, the experimental data and the COSMO-RS prediction calculations.

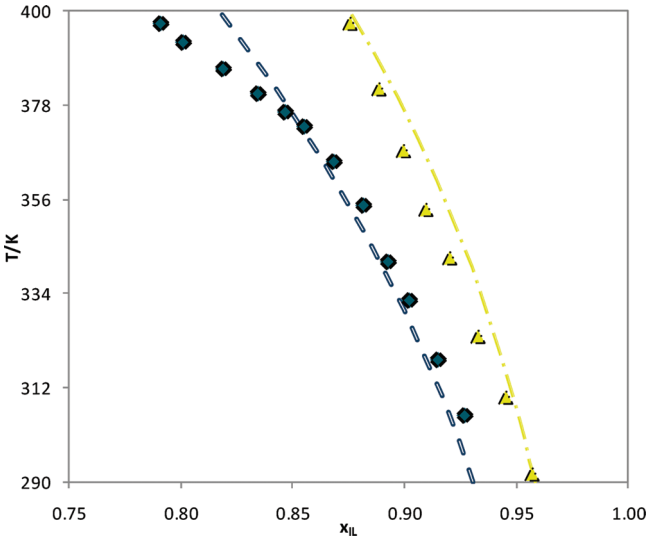

Figure 15. Liquid−liquid phase diagram for $[C_6mim][SCN]$ with cyclohexane[38] (dark blue circles, double dashed line) and cycloheptane[38] (yellow triangles, dot-dashed lines). The symbols and the lines represent, respectively, the experimental data and the COSMO-RS prediction calculations.

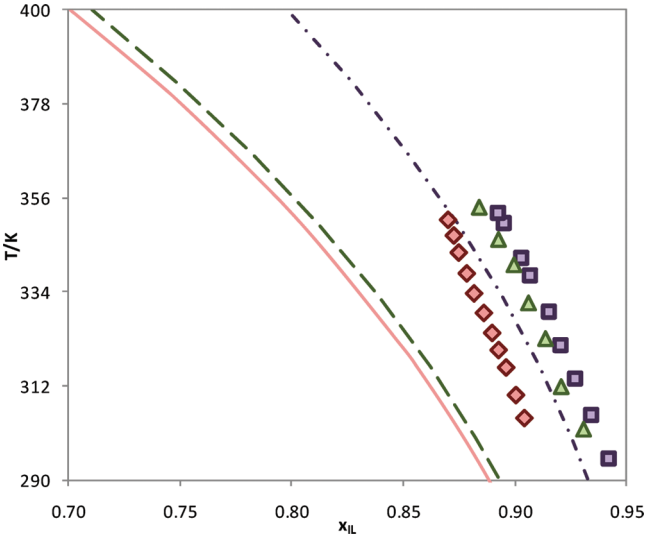

Figure 16. Liquid−liquid phase diagram for $[C_4mim][CF_3SO_3]$[50] (purple squares, dot-dash line), $[C_4mpyr][CF_3SO_3]$[50] (green triangles, long dashed line), and $[1,3C_4mpy][CF_3SO_3]$[50] (pink diamonds, solid line) with cyclohexane. The symbols and the lines represent, respectively, the experimental data and the COSMO-RS prediction calculations.

being of the order of 3×10^{-5} (in mole fraction)[36,38,51] for systems for which data are available.

The predictions provided by COSMO-RS for the description of the LLE experimental data for IL + cycloalkanes systems are discussed below.

4.4.1. Effect of the Cycloalkanes Structure upon the Phase Behavior. The cycloalkanes size has an important effect on the solubilities of these compounds in ionic liquids. The immiscibility region increases with the cycloalkanes size (or carbon number increase) as shown in Figure 15. A number of other systems with distinct ionic liquids, yet a similar behavior, are reported in the Supporting Information (Figures S11−S114).

The COSMO-RS predictions can describe correctly the decreased miscibility with the increase of the cycloalkane size. In the most part of the studied examples a fine quantitative description of the data was also achieved.

4.4.2. Effect of the Ionic Liquid Cation Core upon the Phase Behavior. As previously observed for different hydrocarbons, the cycloalkane containing systems do not vary appreciably with the cations based on nitrogen-containing heterocycles, such as the imidazolium-, pyrrolidinium-, and pyridinium-based ionic liquids (Figure 16). Again slightly higher solubilities were observed with the pyridinium-based ionic liquid. Therefore,

the increasing solubility of hydrocarbons in ionic liquids follows the general rank that is independent of the hydrocarbon nature: pyridinium-based > pyrrolidinium-based ≈ imidazolium-based ionic liquids. Other types of cations (such as phosphonium- QJ;and ammonium-based ionic liquids) may however present quite different behaviors. Yet, the experimental data available are too scarce to draw any conclusions concerning this matter.

COSMO-RS can correctly predict the solubility trends experimentally observed in Figure 16 and, as observed for the aromatic hydrocarbons, it predicts a larger difference in solubility between the imidazolium, the pyridinium, and pyrrolidium cations than that observed experimentally.

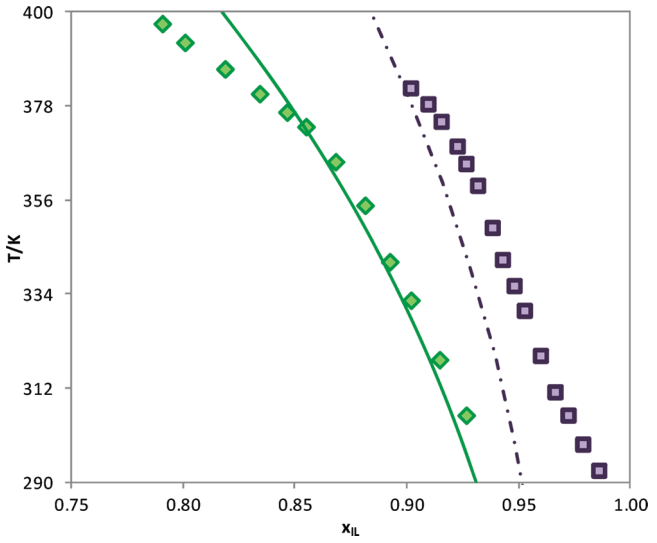

Figure 17. Liquid−liquid phase diagram for $[C_4mim][SCN]$[32] (purple squares, dot-dash line) and $[C_6mim][SCN]$[38] (green diamonds, solid line) with cyclohexane. The symbols and the lines represent, respectively, the experimental data and the COSMO-RS prediction calculations.

4.4.3. Effect of the Ionic Liquid Cation Alkyl Chain Length upon the Phase Behavior. From Figure 17, it can be seen that the increase of the cation alkyl chain length allows dispersive-type interactions between the hydrocarbon and the ionic liquid, which, along with a higher free volume and the favorable packing effect, contribute to an increase in the miscibility between both solvents. Moreover, the replacement of a methyl group by a longer alkoxymethyl group at the ionic liquid cation also leads to a higher solubility of the cyclohexane in the ionic liquid (Supporting Information, Figure S118). In fact, this general trend was observed for the three types of hydrocarbons studied.

Although the experimental data is scarce for a full evaluation of the model, COSMO-RS can provide an excellent quantitative and qualitative description of the systems behavior presented in Figure 17 and Supporting Information, Figure S118.

4.4.4. Effect of the Ionic Liquid Anion upon the Phase Behavior. The experimental data available, reported in Supporting Information Table S3, allow the comparison of the effect of several anions toward the liquid−liquid equilibria with cycloalkanes. Two main examples are displayed in Figure 18 and Supporting Information, Figure S120, for ($[C_4mim]$- and $[C_6H_{13}OCH_2mim]$-based ionic liquids + cyclohexane) binary systems.

The influence of the anion is more relevant in the cycloalkanes solubility in ionic liquids than the cation family effect discussed above. In the $[C_4mim]$-based ionic liquids the miscibility with cyclohexane increases in the order $[SCN]^- < [CF_3SO_3]^- < [MDEGSO_4]^- < [PF_6]^-$. For the $[C_6H_{13}OCH_2mim]$-based ionic liquids the solubility with cyclohexane increases from $[BF_4]^-$ to $[NTf_2]^-$ composing anions. As observed before with *n*-alkanes, these sequences closely follow the solvatochromic β parameter trend (hydrogen bond basicity of the ionic liquid):[66,67] $[SCN]^- > [CF_3SO_3]^- > [MDEGSO_4]^- > [PF_6]^-$.

The COSMO-RS predictions are not completely reliable in describing the ionic liquids anions influence in their mutual solubilities with cycloalkanes, and as previously observed for *n*-alkanes and for aromatic hydrocarbons. The results reported in Figure 18 show that some anions are correctly described, for example, $[SCN]^-$, $[CF_3SO_3]^-$, and $[MDEGSO_4]^-$, while for

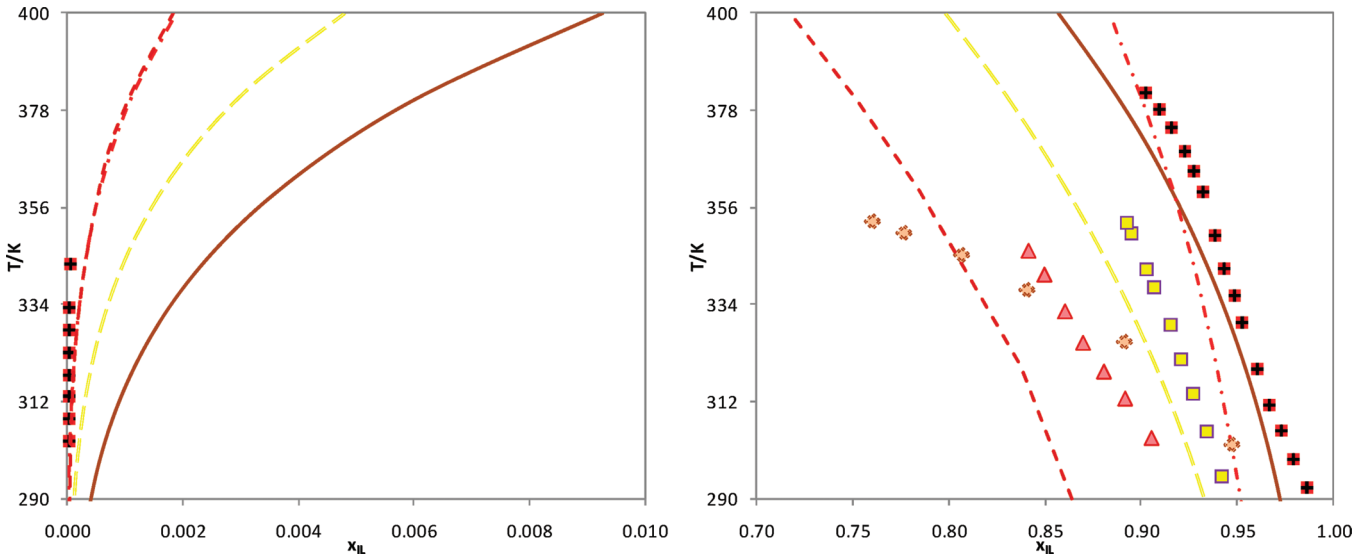

Figure 18. Liquid−liquid phase diagram for $[C_4mim][PF_6]$[51] (orange diamonds, solid line), $[C_4mim][SCN]$[32] (red crossed squares, dot-dash line), $[C_4mim][CF_3SO_3]$[50] (yellow squares, long dashed line) and $[C_4mim][MDEGSO_4]$[39] (pink triangles, short dashed line) with cyclohexane. The symbols and the lines represent, respectively, the experimental data and the COSMO-RS prediction calculations.

dx.doi.org/10.1021/ie102471b |*Ind. Eng. Chem. Res.* 2011, 50, 5279–5294

Table 3. Summary of the Factors That Influence the Solubility and the Performance of COSMO-RS[a]

factor	influence on the solubility	COSMO-RS performance
hydrocarbon type	aromatics ≫ cycloalkanes > *n*-alkanes	Y
	***n*-Alkanes + ILs Systems**	
n-alkane chain length	↑ C_n → ↓ solubility	Y
IL cation core	≈	Y
IL cation alkyl chain length	↑ C_n → ↑ Solubility	Y
IL anion family	$[MeSO_4]^-$ > $[SCN]^-$ > $[TOS]^-$ > $[CF_3SO_3]^-$ > $[MDEGSO_4]^-$ > $[PF_6]^-$ $[BF_4]^-$ > $[NTf_2]^-$	N
IL anion alkyl chain length	↑ C_n → ↑ Solubility	Y
	Aromatics + ILs Systems	
aromatic alkyl chain substituted length	↑ C_n → ↓ Solubility	Y
IL cation core	≈	Y
IL cation alkyl chain length	↑ C_n → ↑ Solubility	Y
IL anion family	$[BF_4]^-$ > $[MeSO_4]^-$ > $[SCN]^-$ > $[EtSO_4]^-$ > $[MDEGSO_4]^-$ > $[TOS]^-$ > $[PF_6]^-$ > $[CF_3SO_3]^-$ > $[NTf_2]^-$	N
IL anion alkyl chain length	↑ C_n → ↑ Solubility	Y
	Cycloalkanes + ILs Systems	
Cycloalkane size	↑ C_n → ↓ Solubility	Y
IL cation core	≈	Y
IL cation alkyl chain length	↑ C_n → ↑ Solubility	Y
IL anion family	$[SCN]^-$ > $[CF_3SO_3]^-$ > $[MDEGSO_4]^-$ > $[PF_6]^-$	N
IL anion alkyl chain length	↑ C_n → ↑ Solubility	Y

[a] Legend: (≈) negligible influence; (Y) COSMO-RS describes the experimental trend correctly; (N) COSMO-RS does not correctly describes the experimental trend.

others, such as $[PF_6]^-$, the model fails in describing their correct trend. COSMO-RS seems to fail with high charge density anions. These anions have stronger Coulombic interactions with the combined cation that are underestimated by the COSMO-RS calculations. Despite these anions, for which the COSMO-RS qualitative description fails, the solubility predictions are correct at least from a semiquantitative point of view, and for some anions, even a close quantitative description is achieved.

4.5. Summary of the Various Effects Studied upon the Phase Behavior. The influence of various factors studied on this work through the mutual solubilities of hydrocarbons and ionic liquids is summarized in Table 3, along with the performance of the COSMO-RS model toward the description of the experimentally observed trends. With the exception of the ionic liquid anion nature influence in the solubility behavior, which was not fully captured by the COSMO-RS iterative calculations, the model seems to be able to produce a semiquantitative description of the experimental data. Often, for the most immiscible systems, even an acceptable quantitative prediction of the phase diagrams, although far from the critical point, is achieved. It seems thus that COSMO-RS could be a useful tool for the screening of ionic liquids to be used in processes dealing with hydrocarbons.

Although binary systems can be of use to identify the ionic liquids for which the solubilities of hydrocarbons are quite different, and therefore are potentially interesting for extraction purposes, they provide limited information. To study the application of ionic liquids to perform extractions in more complex real systems, additional studies on ternary systems are required. For that purpose a companion article to this work, dealing with ternary systems of ionic liquids and hydrocarbon mixtures, is under preparation.

5. CONCLUSIONS

The use of ionic liquids in refineries and petrochemical industries requires the knowledge and the complete understanding of the several structural factors that influence the liquid phase behavior of systems containing such fluids. Therefore, an overview of the mutual solubilities of hydrocarbons and ionic liquids was carried out in this work to evaluate both the structural features of the hydrocarbons (chain length and molecular size, aromaticity, positional isomerism, and cyclization) and of the ionic liquids (cation family, cation alkyl chain, and anion nature) upon the phase behavior. The ability of COSMO-RS, a predictive model based on the quantum chemical model combined with statistical thermodynamics, was also evaluated in describing the phase behavior of these binary systems.

Concerning the COSMO-RS predictions it was shown to be possible to achieve a good qualitative and a semiquantitative description of the structural effects of different hydrocarbons and ionic liquids in the mutual solubilities of the studied systems. The only exception appears in the ionic liquid anion influence for which COSMO-RS is not able to fully capture the different ionic liquids inducing behavior. Another limitation of COSMO-RS is the solubility prediction of systems presenting large mutual miscibilities (far from the infinite dilution regime). For less miscible systems (near complete immiscibility), the predicted values are in good quantitative agreement with experimental data. Despite these limitations, the capability of COSMO-RS to predict the LLE of IL + hydrocarbon binary systems suggests that it can be used as an *a priori* tool for the screening of ionic liquids suitable for applications involving hydrocarbons.

■ ASSOCIATED CONTENT

Supporting Information. Supplementary data, figures, and tables as described in the text. This material is available free of charge via the Internet at http://pubs.acs.org.

■ AUTHOR INFORMATION

Corresponding Author
*E-mail: jcoutinho@ua.pt.

■ ACKNOWLEDGMENT

Ana R. Ferreira acknowledges the financial support from Fundação para a Ciência e a Tecnologia and Galp Energia through the scholarship SFRH/BDE/33835/2009, and Mara G. Freire acknowledges the financial support from Fundação para a Ciência e a Tecnologia through the scholarship SFRH/BPD/41781/2007.

■ REFERENCES

(1) Lu, J.; Yan, F.; Texter, J. Advanced applications of ionic liquids in polymer science. *Prog. Polym. Sci.* **2009**, *34* (5), 431–448.

(2) Zhao, D.; Wu, M.; Kou, Y.; Min, E. Ionic liquids: applications in catalysis. *Catal. Today* **2002**, *74* (1−2), 157–189.

(3) Tian, G.-c.; Li, J.; Hua, Y.-x. Application of ionic liquids in hydrometallurgy of nonferrous metals. *Trans. Nonferrous Met. Soc. Chin.* **2010**, *20* (3), 513–520.

(4) Li, Z.; Jia, Z.; Luan, Y.; Mu, T. Ionic liquids for synthesis of inorganic nanomaterials. *Curr. Opin. Solid State Mater. Sci.* **2008**, *12* (1), 1–8.

(5) Vioux, A.; Viau, L.; Volland, S.; Le Bideau, J. Use of ionic liquids in sol-gel: Ionogels and applications. *C.R. Acad. Sci., Ser. IIc: Chim.* **2010**, *13* (1−2), 242–255.

(6) Meindersma, G. W.; de Haan, A. B., Separation of Aromatic and Aliphatic Hydrocarbons with Ionic Liquids. In *Ionic Liquids: From Knowledge to Application*; American Chemical Society: Washington, DC, 2009; pp 255−272.

(7) Arce, A.; Earle, M. J.; Katdare, S. P.; Rodriguez, H.; Seddon, K. R. Application of mutually immiscible ionic liquids to the separation of aromatic and aliphatic hydrocarbons by liquid extraction: A preliminary approach. *Phys. Chem. Chem. Phys.* **2008**, *10* (18), 2538–2542.

(8) Bélafi-Bakó, K.; Dörmõ, N.; Ulbert, O.; Gubicza, L. Application of pervaporation for removal of water produced during enzymatic esterification in ionic liquids. *Desalination* **2002**, *149* (1−3), 267–268.

(9) Shiflett, M. B.; Yokozeki, A. Separation of carbon dioxide and sulfur dioxide using room-temperature ionic liquid [bmim][$MeSO_4$]. *Energy Fuels* **2009**, *24* (2), 1001–1008.

(10) Yokozeki, A.; Shiflett, M. B. Hydrogen purification using room-temperature ionic liquids. *Appl. Energy* **2007**, *84* (3), 351–361.

(11) Kubisa, P. Ionic liquids as solvents for polymerization processes —Progress and challenges. *Prog. Polym. Sci.* **2009**, *34* (12), 1333–1347.

(12) Werner, S.; Haumann, M.; Wasserscheid, P. Ionic Liquids in Chemical Engineering. *Annu. Rev. Chem. Biomol. Eng.* **2010**, *1* (1), 203–230.

(13) Olivier-Bourbigou, H.; Magna, L.; Morvan, D. Ionic liquids and catalysis: Recent progress from knowledge to applications. *Appl. Catal., A* **2010**, *373* (1−2), 1–56.

(14) Rogers, R. D.; Seddon, K. R. Ionic Liquids—Solvents of the future?. *Science* **2003**, *302* (5646), 792–793.

(15) Seddon, K. R. Ionic liquids: A taste of the future. *Nat. Mater.* **2003**, *2* (6), 363–365.

(16) BASF, The BASIL process: Acid scavenging http://www.basionics.com/en/ionic-liquids/processes/acid.htm (accessed 29/11/2010).

(17) Favre, F.; Forestiere, A.; Hugues, F.; Olivier-Bourbigou, H.; Chodorge, J. A. From monophasic Dimersol (TM) to biphasic Difasol (TM). *Oil Gas-European Magazine* **2005**, *31* (2), 83–87.

(18) Chauvin, Y.; Olivier, H.; Wyrvalski, C. N.; Simon, L. C.; de Souza, R. F. Oligomerization of *n*-Butenes Catalyzed by Nickel Complexes Dissolved in Organochloroaluminate Ionic Liquids. *J. Catal.* **1997**, *165* (2), 275–278.

(19) Li, H. M.; Jiang, X.; Zhu, W. H.; Lu, J. D.; Shu, H. M.; Yan, Y. S. Deep oxidative desulfurization of fuel oils catalyzed by decatungstates in the ionic liquid of Bmim PF_6. *Ind. Eng. Chem. Res.* **2009**, *48* (19), 9034–9039.

(20) Arce, A.; Francisco, M.; Soto, A. Evaluation of the polysubstituted pyridinium ionic liquid [hmmpy][Ntf2] as a suitable solvent for desulfurization: Phase equilibria. *J. Chem. Thermodyn.* **2010**, *42* (6), 712–718.

(21) Gao, H. S.; Guo, C.; Xing, J. M.; Zhao, J. M.; Liu, H. Z. Extraction and oxidative desulfurization of diesel fuel catalyzed by a Bronsted acidic ionic liquid at room temperature. *Green Chem.* **2010**, *12* (7), 1220–1224.

(22) Kuhlmann, E.; Haumann, M.; Jess, A.; Seeberger, A.; Wasserscheid, P. Ionic liquids in refinery desulfurization: Comparison between biphasic and supported ionic liquid phase suspension processes. *Chemsuschem* **2009**, *2* (10), 969–977.

(23) Francisco, M.; Arce, A.; Soto, A. Ionic liquids on desulfurization of fuel oils. *Fluid Phase Equilib.* **2010**, *294* (1−2), 39–48.

(24) Wu, Z. L.; Ondruschka, B. Ultrasound-assisted oxidative desulfurization of liquid fuels and its industrial application. *Ultrason. Sonochem.* **2010**, *17* (6), 1027–1032.

(25) Pereiro, A. B.; Rodriguez, A. Application of the ionic liquid Ammoeng 102 for aromatic/aliphatic hydrocarbon separation. *J. Chem. Thermodyn.* **2009**, *41* (8), 951–956.

(26) Arce, A.; Earle, M. J.; Rodriguez, H.; Seddon, K. R.; Soto, A. Bis{(trifluoromethyl)sulfonyl}amide ionic liquids as solvents for the extraction of aromatic hydrocarbons from their mixtures with alkanes: Effect of the nature of the cation. *Green Chem.* **2009**, *11* (3), 365–372.

(27) Poole, C. F.; Poole, S. K. Extraction of organic compounds with room temperature ionic liquids. *J. Chromatogr. A* **2010**, *1217* (16), 2268–2286.

(28) Lei, Z.; Li, C.; Chen, B. Extractive Distillation: A Review. *Sep. Purif. Rev.* **2003**, *32* (2), 121–213.

(29) Wytze Meindersma, G.; Podt, A.; de Haan, A. B. Selection of ionic liquids for the extraction of aromatic hydrocarbons from aromatic/aliphatic mixtures. *Fuel Process. Technol.* **2005**, *87* (1), 59–70.

(30) Bendová, M.; Wagner, Z. Thermodynamic description of liquid−liquid equilibria in systems 1-ethyl-3-methylimidazolium ethylsulfate + C7-hydrocarbons by polymer-solution models. *Fluid Phase Equilib.* **2009**, *284* (2), 80–85.

(31) Domańska, U.; Laskowska, M.; Marciniak, A. Phase equilibria of (1-ethyl-3-methylimidazolium ethylsulfate plus hydrocarbon, plus ketone, and plus ether) binary systems. *J. Chem. Eng. Data* **2008**, *53* (2), 498–502.

(32) Domańska, U.; Laskowska, M.; Pobudkowska, A. Phase Equilibria Study of the Binary Systems (1-Butyl-3-methylimidazolium Thiocyanate Ionic Liquid plus Organic Solvent or Water). *J. Phys. Chem. B* **2009**, *113* (18), 6397–6404.

(33) Domańska, U.; Pobudkowska, A.; Eckert, F. Liquid-liquid equilibria in the binary systems (1,3-dimethylimidazolium, or 1-butyl-3-methylimidazolium methylsulfate plus hydrocarbons). *Green Chem.* **2006**, *8* (3), 268–276.

(34) Domańska, U.; Zolek-Tryznowska, Z.; Krolikowski, M. Thermodynamic phase behavior of ionic liquids. *J. Chem. Eng. Data* **2007**, *52*, 1872–1880.

(35) García, J.; Torrecilla, J. S.; Fernández, A.; Oliet, M.; Rodríguez, F. (Liquid + liquid) equilibria in the binary systems (aliphatic, or aromatic hydrocarbons + 1-ethyl-3-methylimidazolium ethylsulfate, or 1-butyl-3-methylimidazolium methylsulfate ionic liquids). *J. Chem. Thermodyn.* **2010**, *42* (1), 144–150.

(36) Domańska, U.; Królikowski, M. Phase equilibria study of the binary systems (1-butyl-3-methylimidazolium tosylate ionic liquid + water, or organic solvent). *J. Chem. Thermodyn.* **2010**, *42* (3), 355–362.

(37) Domańska, U.; Pobudkowska, A.; Wisniewska, A. Solubility and excess molar properties of 1,3-dimethylimidazolium methylsulfate, or 1-butyl-3-methylimidazolium methylsulfate, or 1-butyl-3-methylimidazolium octylsulfate ionic liquids with *n*-alkanes and alcohols: Analysis in terms of the PFP and FBT models. *J. Solution Chem.* **2006**, *35* (3), 311–334.

(38) Domańska, U.; Krlikowska, M.; Arasimowicz, M. Phase equilibria of (1-hexyl-3-methylimidazolium thiocyanate + water, alcohol, or hydrocarbon) binary systems. *J. Chem. Eng. Data* **2010**, *55* (2), 773–777.

(39) Domańska, U.; Marciniak, A. Liquid phase behaviour of 1-butyl-3-methylimidazolium 2-(2-methoxyethoxy)-ethylsulfate with organic solvents and water. *Green Chem.* **2007**, *9* (3), 262–266.

(40) Pereiro, A. B.; Rodriguez, A. Binary mixtures containing OMIM PF6: Density, speed of sound, refractive index and LLE with hexane, heptane and 2-propanol at several temperatures. *Phys. Chem. Liq.* **2008**, *46* (2), 172–184.

(41) Domańska, U.; Marciniak, A. Liquid phase behaviour of 1-hexyloxymethyl-3-methyl-imidazolium-based ionic liquids with hydrocarbons: The influence of anion. *J. Chem. Thermodyn.* **2005**, *37* (6), 577–585.

(42) Domańska, U.; Marciniak, A. Phase behaviour of 1-hexyloxymethyl-3-methyl-imidazolium and 1,3-dihexyloxymethyl-imidazolium based ionic liquids with alcohols, water, ketones and hydrocarbons: The effect of cation and anion on solubility. *Fluid Phase Equilib.* **2007**, *260* (1), 9–18.

(43) Domańska, U.; Bakala, I.; Pernak, J. Phase equilibria of an ammonium ionic liquid with organic solvents and water. *J. Chem. Eng. Data* **2007**, *52* (1), 309–314.

(44) Domańska, U.; Lugowska, K.; Pernak, J. Phase equilibria of didecyldimethylammonium nitrate ionic liquid with water and organic solvents. *J. Chem. Thermodyn.* **2007**, *39* (5), 729–736.

(45) Domańska, U.; Marciniak, A.; Krolikowski, M. Phase equilibria and modeling of ammonium ionic liquid, C2NTf2, solutions. *J. Phys. Chem. B* **2008**, *112* (4), 1218–1225.

(46) Lachwa, J.; Szydlowski, J.; Makowska, A.; Seddon, K. R.; Esperanca, J.; Guedes, H. J. R.; Rebelo, L. P. N. Changing from an unusual high-temperature demixing to a UCST-type in mixtures of 1-alkyl-3-methylimidazolium bis{(trifluoromethyl)sulfonyl}amide and arenes. *Green Chem.* **2006**, *8* (3), 262–267.

(47) Domańska, U.; Paduszynski, K. (Solid + liquid) and (liquid + liquid) phase equilibria measurements and correlation of the binary systems {tri-iso-butyl(methyl)phosphonium tosylate + alcohol, or +hydrocarbon}. *Fluid Phase Equilib.* **2009**, *278* (1−2), 90–96.

(48) Domańska, U.; Mazurowska, L. Solubility of 1,3-dialkylimidazolium chloride or hexafluorophosphate or methylsulfonate in organic solvents: Effect of the anions on solubility. *Fluid Phase Equilib.* **2004**, *221* (1−2), 73–82.

(49) Domańska, U.; Królikowski, M.; Pobudkowska, A.; Letcher, T. M. Phase equilibria study of the binary systems (*N*-butyl-4-methylpyridinium tosylate ionic liquid + organic solvent, or water). *J. Chem. Eng. Data* **2009**, *54* (5), 1435–1441.

(50) Marciniak, A.; Karczemna, E. Influence of cation structure on binary liquid−liquid equilibria for systems containing ionic liquids based on trifluoromethanesulfonate anion with hydrocarbons. *J. Phys. Chem. B* **2010**, *114* (16), 5470–5474.

(51) Domańska, U.; Marciniak, A. Solubility of 1-alkyl-3-methylimidazolium hexafluorophosphate in hydrocarbons. *J. Chem. Eng. Data* **2003**, *48* (3), 451–456.

(52) Domańska, U.; Królikowski, M.; Paduszynski, K. Phase equilibria study of the binary systems (*N*-butyl-3-methylpyridinium tosylate ionic liquid + an alcohol). *J. Chem. Thermodyn.* **2009**, *41* (8), 932–938.

(53) Chen, C.-C.; Simoni, L. D.; Brennecke, J. F.; Stadtherr, M. A. Correlation and prediction of phase behavior of organic compounds in ionic liquids using the nonrandom two-liquid segment activity coefficient model. *Ind. Eng. Chem. Res.* **2008**, *47* (18), 7081–7093.

(54) Domańska, U.; Królikowski, M.; Ramjugernath, D.; Letcher, T. M.; Tumba, K. Phase equilibria and modeling of pyridinium-based ionic liquid solutions. *J. Phys. Chem. B* **2010**, *114* (46), 15011–15017.

(55) Klamt, A.; Eckert, F. COSMO-RS: A novel and efficient method for the a priori prediction of thermophysical data of liquids. *Fluid Phase Equilib.* **2000**, *172* (1), 43–72.

(56) Klamt, A., Summary, limitations, and perspectives. In *COSMO-RS*, Elsevier: Amsterdam, The Netherlands, 2005; 205−207.

(57) Diedenhofen, M.; Klamt, A. COSMO-RS as a tool for property prediction of IL mixtures—A review. *Fluid Phase Equilib.* **2010**, *294* (1−2), 31–18.

(58) Klamt, A.; Eckert, F.; Arlt, W. COSMO-RS: An alternative to simulation for calculating thermodynamic properties of liquid mixtures. *Annu. Rev. Chem. Biomol. Eng.* **2010**, *1* (1), 101–122.

(59) Klamt, A., *COSMO-RS from quantum chemistry to fluid phase thermodynamics and drug design*: Elsevier: Amsterdam, The Netherlands, 2005.

(60) Freire, M. G.; Carvalho, P. J.; Santos, L. M. N. B. F.; Gomes, L. R.; Marrucho, I. M.; Coutinho, J. A. P. Solubility of water in fluorocarbons: Experimental and COSMO-RS prediction results. *J. Chem. Thermodyn.* **2010**, *42* (2), 213–219.

(61) Freire, M. G.; Santos, L. M. N. B. F.; Marrucho, I. M.; Coutinho, J. A. P. Evaluation of COSMO-RS for the prediction of LLE and VLE of alcohols + ionic liquids. *Fluid Phase Equilib.* **2007**, *255* (2), 167–178.

(62) Ahlrichs, R.; Bär, M.; Häser, M.; Horn, H.; Kölmel, C. Electronic structure calculations on workstation computers: The program system turbomole. *Chem. Phys. Lett.* **1989**, *162*, 165–169.

(63) Schäfer, A.; Klamt, A.; Sattel, D.; Lohrenz, J. C. W.; Eckert, F. COSMO implementation in TURBOMOLE: Extension of an efficient quantum chemical code towards liquid systems. *Phys. Chem. Chem. Phys.* **2000**, *2* (10), 2187–2193.

(64) Schäfer, A.; Huber, C.; Ahlrichs, R. Fully optimized contracted gaussian basis sets of triple zeta valence quality for atoms Li to Kr. *J. Chem. Phys.* **1994**, *100* (8), 5829–5835.

(65) Freire, M. G.; Ventura, S. P. M.; Santos, L. M. N. B. F.; Marrucho, I. M.; Coutinho, J. A. P. Evaluation of COSMO-RS for the prediction of LLE and VLE of water and ionic liquids binary systems. *Fluid Phase Equilib.* **2008**, *268* (1−2), 74–84.

(66) Lungwitz, R.; Spange, S. A hydrogen bond accepting (HBA) scale for anions, including room temperature ionic liquids. *New J. Chem.* **2008**, *32* (3), 392–394.

(67) Lungwitz, R.; Strehmel, V.; Spange, S. The dipolarity/polarisability of 1-alkyl-3-methylimidazolium ionic liquids as function of anion structure and the alkyl chain length. *New J. Chem.* **2010**, *34* (6), 1135–1140.

(68) Shang, H. T.; Wu, J. S.; Zhou, Q.; Wang, L. S. Solubilities of benzene, toluene, and xylene isomers in 1-butyl-3-methylimidazolium tetrafluoroborate. *J. Chem. Eng. Data* **2006**, *51* (4), 1286–1288.

(69) Arce, A.; Earle, M. J.; Rodriguez, H.; Seddon, K. R.; Soto, A. 1-Ethyl-3-methylimidazolium bis{(trifluoromethyl)sulfonyl}amide as solvent for the separation of aromatic and aliphatic hydrocarbons by liquid extraction−extension to C7- and C8-fractions. *Green Chem.* **2008**, *10* (12), 1294–1300.

(70) Domańska, U.; Pobudkowska, A.; Królikowski, M. Separation of aromatic hydrocarbons from alkanes using ammonium ionic liquid C2NTf2 at T = 298.15 K. *Fluid Phase Equilib.* **2007**, *259* (2), 173–179.

(71) Blesic, M.; Lopes, J. N. C.; Gomes, M. F. C.; Rebelo, L. S. P. N. Solubility of alkanes, alkanols, and their fluorinated counterparts in tetraalkylphosphonium ionic liquids. *Phys. Chem. Chem. Phys.* **2010**, *12* (33), 9685–9692.

(72) Shiflett, M. B.; Niehaus, A. M. S. Liquid−liquid equilibria in binary mixtures containing substituted benzenes with ionic liquid 1-ethyl-3-methylimidazolium bis(trifluoromethylsulfonyl)imide. *J. Chem. Eng. Data* **2009**, *55* (1), 346–353.

(73) Dreiseitlová, J.; Řehák, K.; Vreekamp, R. Mutual solubility of pyridinium-based tetrafluoroborates and toluene. *J. Chem. Eng. Data* **2010**, *55* (9), 3051–3054.